EXPERIMENTAL STUDY OF THE INTERACTION OF A LASER PLASMA FLOW WITH A TRANSVERSE MAGNETIC FIELD

A. A Soloviev, K. F Burdonov, A. V Kotov, S. E Perevalov, R. S Zemskov, V.N. N Ginzburg, A. A Kochetkov, A. A Kuzmin, A. A Shaikin, I. A Shaikin, et al.

EXPERIMENTAL STUDY OF THE INTERACTION OF A LASER PLASMA FLOW WITH A TRANSVERSE MAGNETIC FIELD

A. A. Soloviev[1], K. F. Burdonov[1], A. V. Kotov[1], S. E. Perevalov[1], R. S. Zemskov[1], V. N. Ginzburg[1], A. A. Kochetkov[1], A. A. Kuzmin[1], A. A. Shaikin[1], I. A. Shaikin[1], E. A. Khazanov[1], I. V. Yakovlev[1], A. G. Luchinin[1], M. V. Morozkin[1], M. D. Proyavin[1], M. Yu. Glyavin[1], J. Fuchs[2], and M. V. Starodubtsev[1]

Abstract

We present the results of studying experimentally the expansion of laser plasma in a strong external magnetic field (with a magnetic flux density of 13.5 T) at various sizes of the region of plasma formation on the surface of a solid-state target. It is shown that when the size of the plasma formation region is smaller than the classical plasma braking radius, a nearly identical topology of plasma flows is observed, which is characterized by the formation of a thin plasma sheet directed along the external magnetic field. If the width of the plasma formation region is comparable with the classical plasma braking radius, an additional plasma sheet starts to be formed.

Introduction

Studies of the interaction of laser plasma with external magnetic fields opens up ample opportunities in the context of various magnetohydrodynamic and wave processes, as well as their application to solution of many fundamental and applied problems. Interest in such works is largely related to the problems of laser-plasma acceleration of charged particles and control of their characteristics [1–4], development of new schemes for generation of secondary emissions [5–10], etc. At the same time, strong external magnetic fields are actively used in physics of high energy densities. Here, the processes of interaction of laser plasma with magnetic fields open up broad options of studying experimentally a wide spectrum of problems, from improving the efficiency of target heating during controlled fusion using a strong external magnetic field [11– 16] to modeling astrophysical phenomena in the laboratory [17–24]. For example, when accretion of matter to young stars is modeled, one can successfully employ laboratory experiments with the use of high-speed flows of the laser plasma produced by nanosecond laser pulses that impact solid-state targets located in an external magnetic field [20–24].

Laboratory modeling allows one to solve a number of important astrophysical problems. In particular, the methods of modeling numerically the process of matter fall from the accretion disk onto a young star cannot provide a comprehensive answer to the question about the structure of the transition zone between the inner edge of the accretion disk and the magnetosphere of the star. As a result, there exist several, noticeably different models that describe this process, including the models of accretion along magnetic field lines [25–28] and accretion in the equatorial plane of the star [29–30], which is due to the development of the Rayleigh–Taylor instability. In this case, laboratory experiments make it possible to reveal, which physical processes play the determining role in the transition zone, develop the corresponding numerical model of interaction of the moving plasma with the ambient magnetic field, and use it as a basis for estimating the main parameters of both the plasmas in the accretion disk at the magnetosphere boundary and the flows inside the accretion column.

Due to the fact that the transition zone between the inner edge of the accretion disk and the magnetosphere of the star is characterized by the rough balance of the gas-dynamic plasma pressure and the magnetic pressure, fulfillment of this condition is the main requirement in the development of the experiment scheme. To estimate the characteristic parameters of the laser plasma under these conditions, one can use the so-called classical plasma braking radius [31,32]

$$R_b \sim \left(3E_0 / B_0^2\right)^{1/3} \quad (1)$$

Then it is assumed that the laser plasma with the total energy E_0 is produced instantly at a certain point of space with a uniform external magnetic field B_0, after which it expands isotropically with the initial supersonic velocity V_0. Due to its high conductivity, the laser plasma pushes the magnetic field out of its volume and reaches the size of about R_b till the time when it ceases to move completely. The average plasma density inside the sphere with the radius R_b turns to be about

$$\langle N \rangle \sim \frac{E_0}{V_0^2 M \left(\frac{4\pi}{3}\right) R_b^3} \sim \frac{B_0^2}{4\pi V_0^2 M} \quad (2)$$

where M is the ion mass. One can see that the quantity <N> does not depend on the energy of the laser pulse and is determined by the ratio of the magnetic flux density B0 of the external magnetic field to the initial ion velocity V_0. It should be noted that in most experiments performed to study the spread of the laser plasma produced by irradiating solid-state targets with nanosecond laser pulses [17–24], the characteristic values of V_0 turn out to be rather close and lying in the range from 100 to 500 km/s, despite the noticeably different parameters of the laser radiation (e.g., its intensity on the target surface changes from $I \sim 10^{11}$ W/cm^2 [17, 18] to $I \sim 10^{13}$–10^{14} W/cm^2 [20–24]). Thus, the influence of the magnetic flux density B_0 of the external magnetic field on the average plasma density turns out to be determining.

A significant part of the experiments on the interaction of laser plasma flows with an external magnetic field is performed using large-scale experimental facilities with characteristic scales of the external magnetic field about 1 m and a magnetic flux density of about 100–1000 G (0.01–0.10 T) [18, 19]. In this case (for laser pulse energies of 10–100 J), the characteristic dimensions Rb turn out to be about tens of centimeters, and the average densities <N>, of the order of 10^{14} cm^{-3}. It should be noted that the use of such an approach limits the geometry of the experiments to a certain degree, so that the size of the laser plasma source is always much smaller than R_b and the quasispherical plasma spread into the uniform external magnetic field is studied.

A different approach to studying the processes of interaction of laser plasma with an external magnetic field, which is realized with the PEARL facility at the Institute of Applied Physics (IAP) of the Russian Academy of Sciences, is based on the use of much stronger magnetic fields (more than 10 T). In this case, the characteristic dimensions R_b prove to be about 3 mm, and the average plasma densities, about 10^{18} cm^{-3} for a characteristic laser pulse energy of 10 J. Let us indicate the main advantages of this approach based on the use of stronger magnetic fields. First, it is seen that the obtained values of R_b and <N> make it possible to use optical methods of diagnostics, such as, e.g., femtosecond laser interferometry, which allows making instantaneous two-dimensional snapshots of the electron number density distribution in the flow of spreading laser plasma with high spatial and temporal resolution. Second, the small size of R_b allows one to vary the experiment geometry significantly, including the possibility to create a laser-plasma source with dimensions of the order of or even larger than R_b, which offers an opportunity to extend significantly the geometry of the experiments on interaction of plasma flows with an external magnetic field.

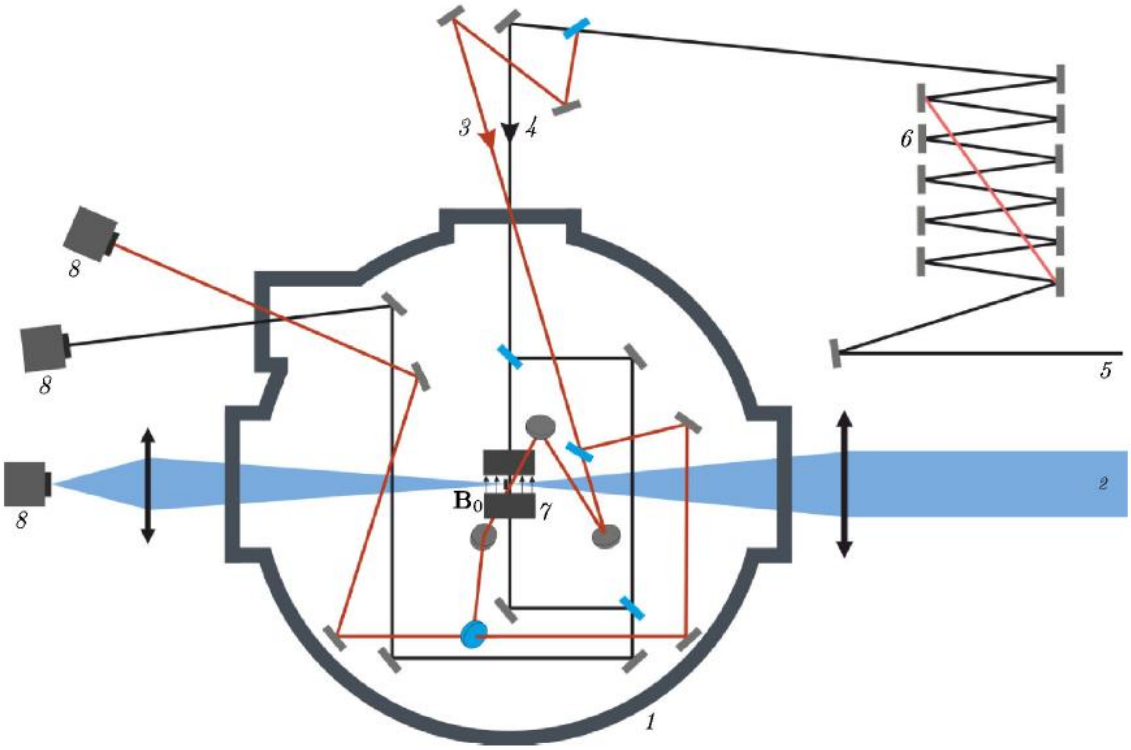

Fig. 1. Setup of the experiment: target chamber (1), pumping laser (2), vertical and horizontal components (3 and 4, respectively) of the diagnostic laser beam (5), delay line (6), coils (7), and CCD cameras (8).

In this work, we study the influence of the size of the laser spot on the target surface on the structure of the plasma flow, which expands into a homogeneous external magnetic field, in the case where this size is less than or comparable with the classical plasma braking radius R_b. In particular, the obtained experimental data on the topology of the laser-plasma flow are presented for the first time for the laser-spot size approximately equal to R_b.

Setup of the experiment

The experiments were performed on a laboratory facility for studies of laser-plasma interaction [33, 34] based on the PEARL laser complex [35]. The laser plasma was produced inside the magnetic system described in Sec. 2.2.

A schematic diagram of the experiment is shown in Fig. 1. To produce the plasma, we used the second harmonic of the PEARL pumping laser shown in blue in Fig. 1 (N_d glass laser [36] with a pulse duration of 1 ns, a pulse energy of up to 180 J, a wavelength of 527 nm, and the beam diameter D = 10 cm). The laser pulse was focused on a solid-state target, which was installed inside the magnetic system, by using a lens with the focal distance F = 1 m. The diameter of the spot on the target could vary from 0.1 to 2 mm, and the radiation intensity in this case fell within the range $2 \cdot 10^{11}$–10^{14} W/cm^2. Under the action of this radiation, a high-speed (100–500 km/s) plasma flow with a density of about 10^{18} cm^{-3} was produced, which was spreading in vacuum mainly in the direction perpendicular to the target surface.

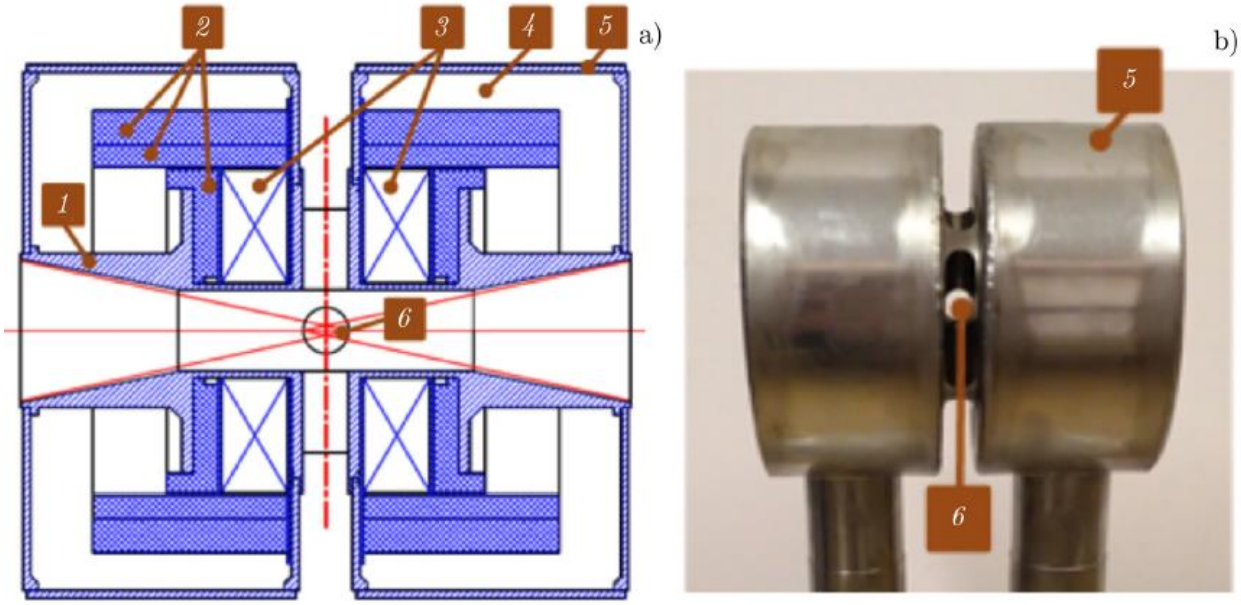

Fig. 2. Sectional schematic (a) and a general view (b) of the magnetic system: metal load-bearing frame (1), composite elements of the frame (2), windings (3), nitrogen chamber (4), external shield (5), and tapered openings for input of the laser radiation and output of the plasma flow.

To model the processes of interaction of high-speed plasma flows with an external magnetic field, the target chamber was equipped with a magnetic system in the form of Helmholtz coils, which made it possible to input the pumping and test laser radiation (see Fig. 2). The maximum magnetic flux density of the external magnetic field at the coil center can reach about 20 T.

Since laser plasma experiments are performed in a target chamber at a pressure of residual gases lower than 10^{-5} Torr and the pulse repetition rate can be up to one pulse per several minutes, a cryostat filled with liquid nitrogen is used to cool down the coils of the magnetic system. The magnetic system created for experiments on the laser-plasma PEARL facility, consists of a pair of coils with a distance of about 1cm between them, which are fixed in a vacuum-tight box with double walls, between which liquid nitrogen is poured. The design of the body, along with the mechanical strength and vacuum tightness, makes it possible to

(1) install the target inside a coil with the possibility of fine tuning of the target position;
(2) ensure a gap at least 2 cm wide in mutually perpendicular directions for the diagnostic radiation;

(3) input the high-power laser radiation in a wide range of angles relative to the direction of the magnetic field.

The necessity of focusing the high-power laser radiation inside the magnetic system imposes an additional requirement on the design of the system: structural elements should not impede the focusing (including point beam focusing) of the laser radiation at the center of the magnetic system. The magnetic system of the PEARL facility ensures the maximum focusing $D/F \leq 1/5$ in the direction across the external magnetic field and $D/F \leq 1/4$, in the longitudinal direction. It also ensures uniformity of the magnetic flux density in the gap between the coils at the level about $\Delta B_0/B_0 \sim 10$ %, which is quite sufficient for experiments on expansion of nanosecond laser plasma into the external magnetic field. The requirements for the uniformity of the magnetic flux density are not very rigid, since in any case the field is perturbed strongly by the plasma flow.

The magnetic field was produced by a discharge of the capacitor unit through a coil. The time of arrival of the laser pulse at the target was synchronized with the peak of the discharge, when the field in the coil was the strongest. The characteristic duration of the discharge is several milliseconds, which is much longer than the characteristic duration of the dynamics of the studied laser plasma (less than or approximately equal to 100 ns). Therefore, the magnetic field can be regarded constant for the duration of the experiments on expansion of the laser plasma.

As has been noted above, the design of the magnetic system consisting of two Helmholtz coils made it possible to install targets inside the uniformity region of the magnetic field, input high-power plasma-generating laser pulses to this region, and examine the region occupied by the laser plasma with the help of two mutually perpendicular collimated diagnostic femtosecond laser beams with diameters of about 2 cm, thus providing the possibility to obtain instantaneous 2D interferometric snapshots of the laser plasma in two direction simultaneously, namely, along and across the external magnetic field (see Fig. 3).

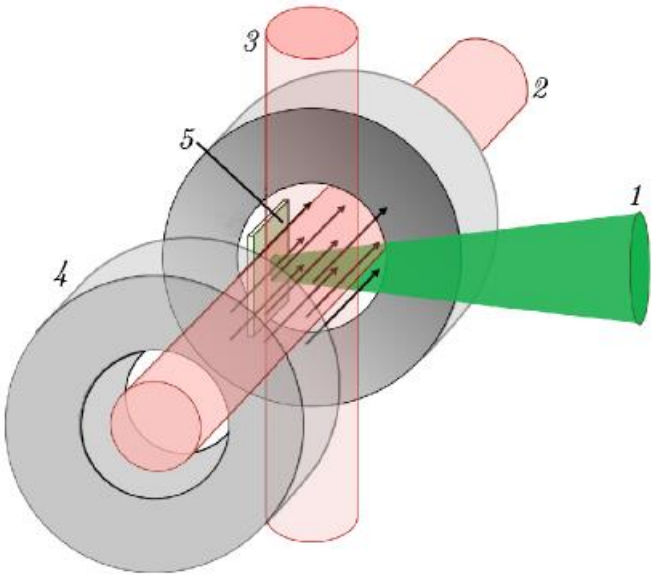

Fig. 3. Scheme of the positions of the plasmagenerating nanosecond (1) and probing femtosecond (2 and 3) laser beams in the magnetic system (4 is the winding and 5 is the target).

The targets were installed approximately normally to the direction of the plasma-generating nanosecond laser pulse. They were rectangular plates of CF_2 Teflon (with dimensions of about 5 × 10 × 1 mm) connected to a glass tube fixed on a motor-driven positioning system, which was installed specially for this series of experiments. This system allowed us to place the target in the plane, which ensured the required intensity of the laser pulse on the target surface, and move the target to a new point after each shot. This allowed us to run off a series of shots using one target with no need for breaking the vacuum in the target chamber to replace the target after each shot.

The plasma was diagnosed by the method of femtosecond optical interferometry using the PEARL laser radiation at the output of the optical compressor with a central wavelength of 910 nm, a duration of less than 100 fs, and an energy of up to 10 mJ. Two Mach–Zehnder interferometers (horizontal and vertical, which are shown black and brown, respectively, in Fig. 1), have been assembled in the target chamber. They allowed us to use the delay line (see Fig. 1) to collect information about the phase distortions in the plasma at times from 8 to 108 ns after the start of formation of the plasma cloud in two planes: along the magnetic field (vertical interferometer) and perpendicularly to it (horizontal interferometer). Glan prisms were used to divide a femtosecond beam in space into two polarization components, one of

which was delayed for 10 ns relative to the other, which allowed us to study two different moments of plasma evolution during one shot. A set of instantaneous snapshots of the plasma in the process of its interaction with an external magnetic field, which is obtained by this method, provides comprehensive information about the studied processes.

Experimental results

Figure 4 shows interferograms of the laser plasma spreading into the external magnetic field B_0 = 13.5 T. The characteristic time of the spread of the plasma cloud up to the size R_b, when it should be stopped under the pressure of the external magnetic field, is about $\tau b \sim R_b/V_0 \sim 8$ ns. Several characteristic stages are discerned in the dynamics of the interaction of the plasma flow with the magnetic field. At the initial stage (at times much shorter than τ_b), the external magnetic field does not affect the plasma spread. In this case, the plasma flow is characterized by a greater ratio $2\mu_0\rho_0V_0/B_0^2 \sim 10^3$ of the gas-dynamic pressure into the magnetic pressure (here, μ_0 is the magnetic constant and ρ_0 is the plasma density). At times of the order of τ_b, the plasma reaches the size of the order of R_b, and its spread is stopped by the magnetic pressure (see Fig. 4a). In this case, the magnetic lines are distorted, and a sufficiently sharp boundary is formed between the plasma cloud and the magnetic field. The Rayleigh–Taylor magnetic instability (flute instability; see the inset in Fig. 4a and also the detailed description of this process in [20]) starts developing at this boundary. At longer times, the plasma flow as a whole is directed to the upper part of the plasma cloud, where a thin plasma sheet is formed, which is strongly compressed in the direction across the external magnetic field (see Fig. 4b) and stretched along the magnetic field (this geometry of the flow is confirmed by interferograms, which are measured across B_0, but not presented here; thus, the fine structure observed in the top part of Figs. 4b–4d is a projection of the plasma sheet oriented perpendicularly to the observation plane). Further, the plasma cloud is compressed by the pressure of the magnetic field and the plasma is predominantly displaced along this plasma sheet (see Figs. 4c–4e). The experimental data show that the characteristic scale of the flute instability increases as the plasma cloud expands (cf. insets in Figs 4a and 4b, as well as the structure of the side lobes in Figs. 4c–4e).

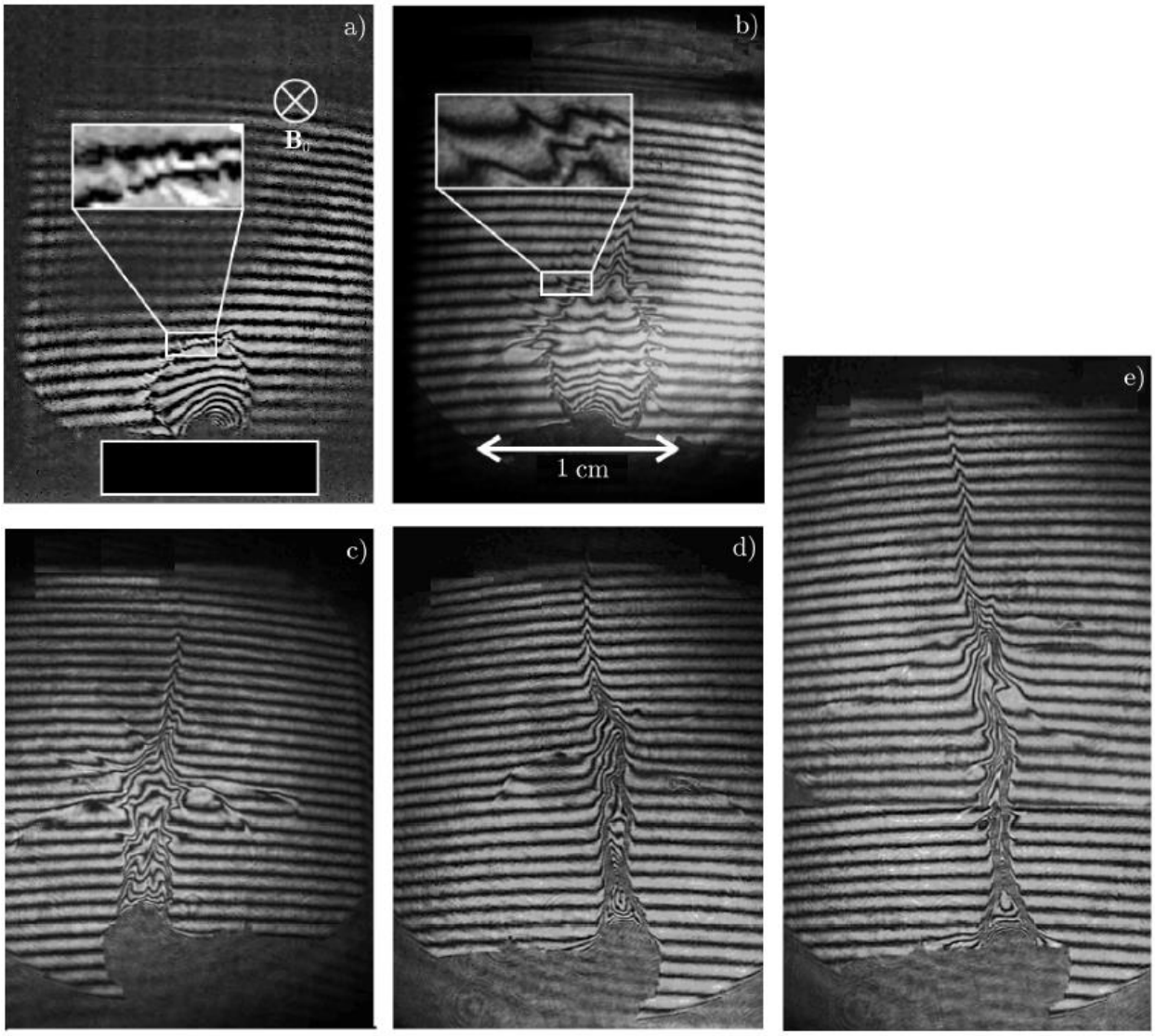

Fig. 4. Dynamics of the spread of laboratory plasma into an external magnetic field with a magnetic flux density of 13.5 T for time instants 8 ns~ τ_b (a), 18 ns (b), 28 ns (c), 38 ns (d), and 48 ns (e). The rectangle at the bottom of panel a denotes the target.

The above-described process of the interaction of a laser plasma with a magnetic field was studied comprehensively in [22], and its initial stage (corresponding to Fig. 3a) was also studied well in experiments on large-scale facilities [18, 19]. However, the experimental data presented in [18, 19, 22] were obtained for the laser plasma source, whose dimensions were much smaller than the radius Rb of plasma braking by the magnetic field. In this work, we present the first experimental data using a source of laser plasma with a size approximately equal to R_b.

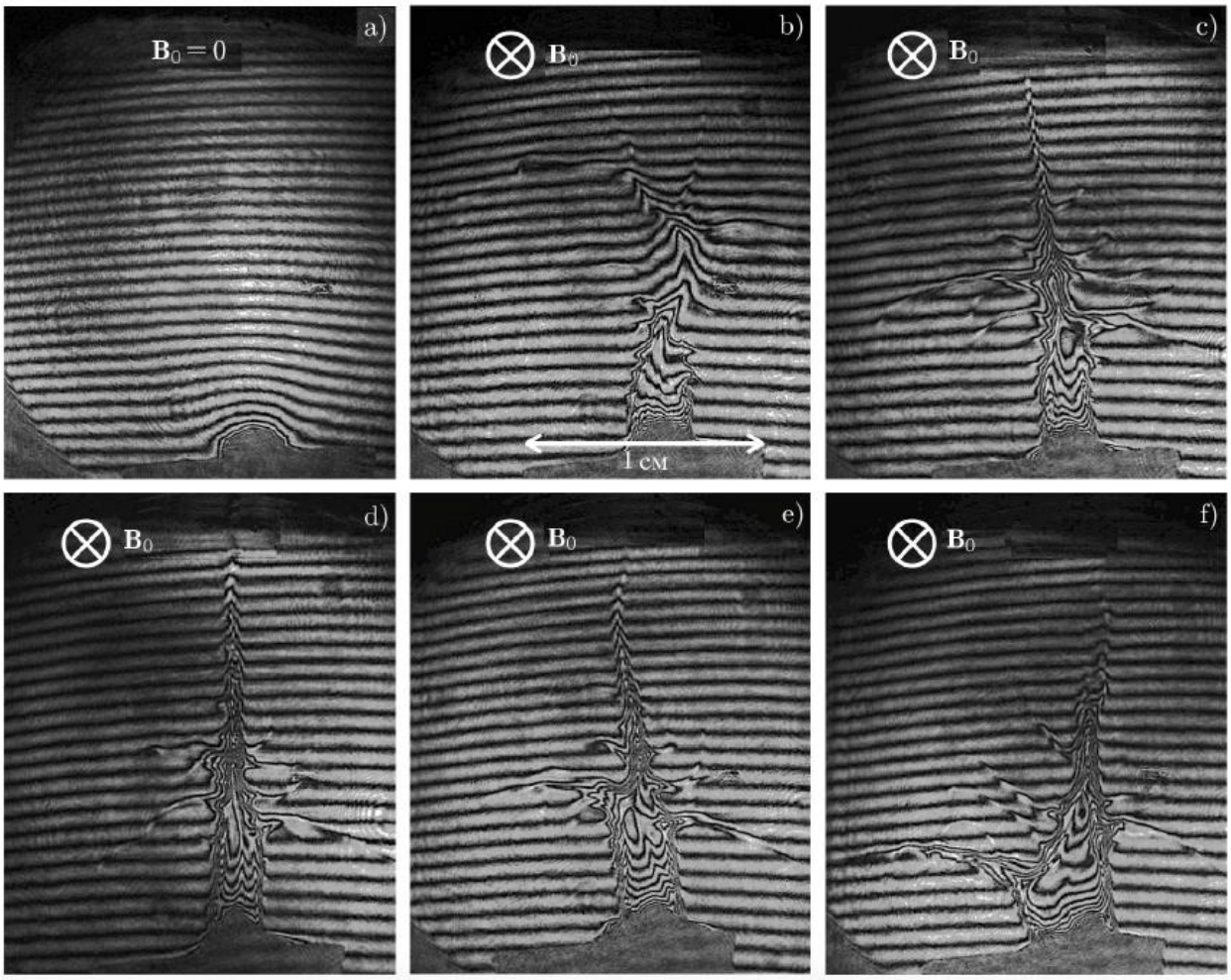

Figure 5 shows interferograms of the laser plasma spreading in the direction across the external magnetic field with a magnetic flux density of 13.5 T for several diameters of the laser spot on the surface of a solid-state target. They are measured in the direction along the magnetic field and allow one to gain understanding of the difference in the regimes of spreading of the laser plasma, as the size of its source varies.

For the sake of comparison, Fig. 5a shows an interferogram of the laser plasma cloud in 28 ns after the end of the plasma-generating laser pulse in the absence of an external magnetic field. One can see that the plasma spreading regime is almost isotropic, which leads to fast spreading of the cloud and the absence of an observable signal already at a distance of several millimeters from the target. Figures 5b–5f show interferograms of the plasma flows in 28 ns after the end of the plasma-generating pulse in the magnetic field with a magnetic flux density of 13.5 T. The time 28 ns is greater than $\tau_b \sim R_b/V_0 \sim 8$ and corresponds to the phase of compression of the plasma cloud under the pressure of the magnetic field and displacement of the plasma in the form of a sheet in the direction perpendicular to the target surface. The interferograms in Figs. 5b–5f correspond to different diameters D of laser spots on the target surface for identical energies of the laser pulse (about 18 J): the value of D increased from about 0.1 mm (Fig. 5b) to 1.8 mm (Fig. 5f). It should be noted that the coefficient of absorption of the laser radiation decreases as the radiation intensity on the target surface increases, but for the data shown in Fig. 4, this coefficient lies in the range from 90% (Fig. 5f) to 70% (Fig. 5b) [37]. Thus, it can be assumed to be almost identical for all the presented interferograms.

Comparison of the interferograms shown in Figs. 5c–5e demonstrates that at small sizes of the plasma source, one observes very similar, nearly indistinguishable topology of plasma flows, which is characterized by a single plasma sheet, which propagates perpendicular to the target surface, and

pronounced side lobes related to the development of Rayleigh–Taylor magnetic instability. As the laser spot on the surface of the solid-state target increases up to sizes of about 2 mm, this topology starts distorting. In particular, it is seen that an additional plasma sheet starts to branch off the target surface, which is well pronounced in the left bottom part of Fig. 5f. This result is evidently novel and requires further detailed experimental and theoretical studies. Additionally, it is interesting to note that the plasma sheet in Fig. 5b, i.e., at a very small size of the laser beam on the target surface (and, correspondingly, at great values of the laser radiation intensity and, apparently, at high plasma temperatures), seems to be less stable than that in Fig. 5c–5e. One can see that the sheet undergoes transverse oscillations and disintegrates into several sheets, as the distance from the target increases. This result also requires further studies.

Discussion and conclusions

In the reported experiments, the dynamics of interaction of the propagating plasma flow with a transverse magnetic field has been studied in detail. The features of plasma penetration into the magnetic field have been studied, and it is shown that even a strong magnetic field (with a magnetic flux denisty of more than 10 T) does not stop the plasma flow in the region where the gas-dynamic and magnetic pressures are identical. On the contrary, the experimental results presented illustrate the complex threedimensional dynamics of the interaction of laser plasma with an external magnetic field. This interaction results in formation of a thin plasma sheet, which is oriented along an external magnetic field and moves away from the target to distances that exceed the dimensions of the laser spot by tens of times. The main mechanism that determines such dynamics of the plasma flow is apparently the Rayleigh–Taylor magnetic instability [22]. The presented experimental results show that if the initial transverse size D of the plasma flow is sufficiently small (noticeably smaller than the braking radius Rb), the flow topology is practically independent of D. At the same time, when the transverse size D is comparable with Rb, the flow topology starts to change. In particular, the start of the formation of an additional plasma layer moving away from the target surface is observed. This experimental result can be significant for the development and testing of numerical models intended to describe the processes of interaction of plasma flows with the magnetic field.

It should be noted that there are other spatial scales in the problem of spreading of laser plasma to the external magnetic field, e.g., the characteristic spatial period λ_{RT} of the Rayleigh–Taylor instability, which is equal to or less than about 1 mm for our experimental parameters [22]. The changes in the topology of the plasma flow, which depend on the ratio between D and λ_{RT}, should be the topic for further studies.

Along with the evident relation of the performed experiments to laboratory astrophysics [20–24], in particular, to the problems of plasma penetration from the accretion disk to the magnetosphere of stars [23], the observed magnetized plasma structures can be of interest in the context of other applications. Indeed, many schemes of laser-plasma sources of accelerated charged particles and secondary emissions require sharp boundaries between the plasma and free space. As an example, one can note the problem of creating a terahertz using a magnetized wakefield wave [5–10], where the sharp boundary between the plasma and free space is required for efficient generation of terahertz radiation. Another example can be the problem of propagation of high-power femtosecond laser pulses in the near-critical plasma in the self-trapping regime [38, 39], which is accompanied by efficient generation of high-charge electron beams and hard betatron radiation. Experimental realization of this regime of the interaction of laser radiation with plasmas requires that the laser pulse should be focused on the sufficiently sharp plasma boundary.

Creation of a plasma target with a sharp boundary is a complex experimental problem. A way to create such targets is to use the considered plasma flows in a strong transverse external magnetic field, which makes it possible to form a sufficiently sharp boundary between the plasma and free space (see Fig. 6) with the characteristic width of the transitional region, which does not exceed 200 μm (the numerical modeling presented in [21] also yielded a close value of the thickness of the transition layer between the plasma and free space.)

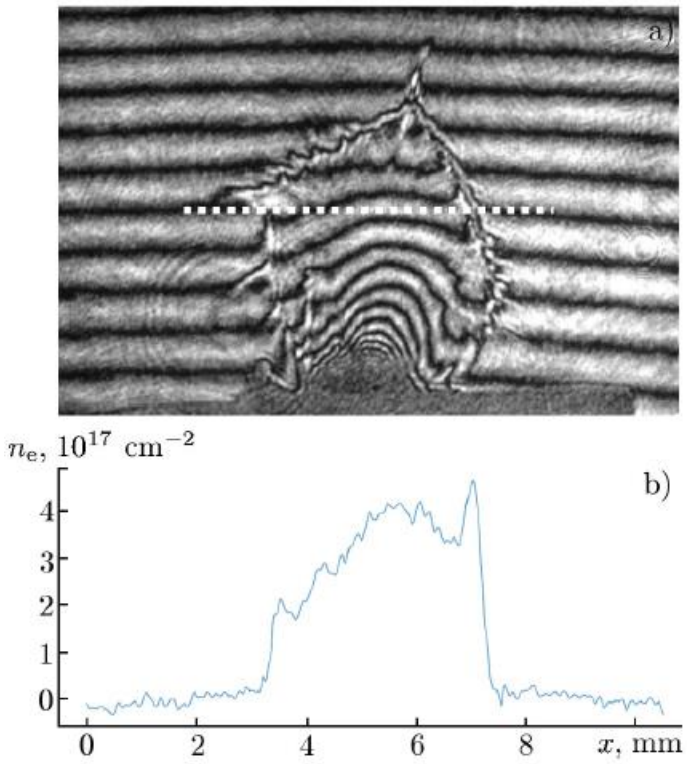

Fig. 6. Interferogram of the plasma cloud interacting with an external magnetic field (B_0 = 13.5 T) in 8 ns after the end of the plasma-generating pulse (a) and the profile of $n_e(x) \equiv \int_{-\infty}^{+\infty} N_e(x,y)\,dy$ (b) which corresponds to the dashed line in panel a, where Ne is the plasma density and the y axis is directed across the plane of the figure in panel a.

Manufacture of the magnetic system was supported by the Russian Science Foundation (project No. 20–12–00395). The experimental study of the regimes of interaction of plasma flows with the magnetic field was supported by the Russian Foundation for Basic Research (project No. 18–29–21029-mk).

References

1. S. Bolanos, J. Beard, G. Revet, et al., Matter Rad. Extremes, 4, 044401 (2019).

https://doi.org/10.1063/1.5082330

2. R. Kodama, K. A. Tanaka, Y. Sentoku, et al., Phys. Rev. Lett., 84, No. 4, 674–677 (2000).

https://doi.org/10.1103/PhysRevLett.84.674

3. S. Rassou, A. Bourdier, and M. Drouin, Phys. Plasmas, 22, No. 7, 073104 (2015).

https://doi.org/10.1063/1.4923464

4. M. Nakatsutsumi, Y. Sentoku, A. Korzhimanov, et al., Nat. Commun., 9, 280 (2018).

https://doi.org/10.1038/s41467-017-02436-w

5. J. Yoshii, C. H. Lai, T. Katsouleas, et al., Phys. Rev. Lett., 79, No. 21, 4194–4197 (1997).

https://doi.org/10.1103/PhysRevLett.79.4194

6. N. Yugami, T. Higashiguchi, H. Gao, et al., Phys. Rev. Lett., 89, No. 6, 065003 (2002).

https://doi.org/10.1103/PhysRevLett.89.065003

7. D. Dorranian, M. Starodubtsev, H. Kawakami, et al., Phys. Rev. E, 68, No. 2, P. 2, 026409 (2003).

https://doi.org/10.1103/PhysRevE.68.026409

8. D. Dorranian, M. Ghoranneviss, M. Starodubtsev, et al., Laser Part. Beams, 23, No. 4, 583–596 (2005).

https://doi.org/10.1017/S0263034605060052

9. D. Dorranian, M. Ghoranneviss, M. Starodubtsev, et al., Phys. Lett. A, 331, Nos. 1–2, 77–83 (2004).

https://doi.org/10.1016/j.physleta.2004.08.027

10. M. I. Bakunov, S. B. Bodrov, A. V. Maslov, and A. M. Sergeev, Phys. Rev. E, 70, No. 1, 016401 (2004).

https://doi.org/10.1103/PhysRevE.70.016401

11. S. Fujioka, Z. Zhang, K. Ishihara, et al., Sci. Rep., 3, 1170 (2013). https://doi.org/10.1038/srep01170

12. P. Y. Chang, G. Fiksel, M. Hohenberger, et al., Phys. Rev. Lett., 107, No. 3, 035006.

https://doi.org/10.1103/PhysRevLett.107.035006

13. D. H. Froula, J. S. Ross, B. B. Pollock, et al., Phys. Rev. Lett., 98, No. 13, 135001 (2007).

https://doi.org/10.1103/PhysRevLett.98.135001

14. L. J. Perkins, B. G. Logan, G. B. Zimmerman, and C. J.Werner, Phys. Plasmas, 20, No. 7,

072708 (2013). https://doi.org/10.1063/1.4816813

15. L. J. Perkins, D. D.-M. Ho, B. G. Logan, et al., Phys. Plasmas, 24, No. 6, 062708 (2017).

https://doi.org/10.1063/1.4985150

16. S. Sakata, S. Lee, H. Morita, et al., Nat. Commun., 9, 3937 (2018).

https://doi.org/10.1038/s41467-018-06173-6

17. C. Plechaty, R. Presura, A. A. Esaulov, Phys. Rev. Lett., 111, No. 18, 185002 (2013).

https://doi.org/10.1103/PhysRevLett.111.185002

18. Yu. P. Zakharov, V. M. Antonov, E. L. Boyarintsev, et al., ´ Plasma Phys. Rep., 32, 183–204 (2006).

https://doi.org/10.1134/S1063780X06030020

19. A. S. Bondarenko, D. B. Schaeffer, E. T. Everson, et al., Nat. Phys., 13, 573–577 (2017).

https://doi.org/10.1038/nphys4041

20. B. Albertazzi, A. Ciardi, M. Nakatsutsumi, et al., Science, 346, No. 6207, 325–328 (2014).

https://doi.org/10.1126/science.1259694

21. G. Revet, S. N. Chen, R. Bonito, et al., Sci. Adv., 3, No. 11, e1700982 (2017).

https://doi.org/10.1126/sciadv.1700982

22. B. Khiar, G. Revet, A. Ciardi, et al., Phys. Rev. Lett., 123, No. 20, 205001 (2019).

https://doi.org/10.1103/PhysRevLett.123.205001

23. E. P. Kurbatov, D. V. Bisikalo, M. V. Starodubtsev, et al., Astron. Rep., 62, No. 8, 483–491 (2018).

https://doi.org/10.1134/S1063772918080061

24. K. Burdonov, G. Revet, R. Bonito, et al., Astron. Astrophys., 642, A38 (2020).

https://doi.org/10.1051/0004-6361/202038189

25. L. Hartmann, Accretion Processes in Star Formation, Cambridge Univ. Press, Cambridge (2008).

26. M. Camenzind, in: G. Klare, ed., Accretion and Winds, Reviews in Modern Astronomy. Vol. 3, Springer,

Berlin–Heidelberg (1990), pp. 234–265. https://doi.org/10.1007/978-3-642-76238-3 17

27. A. Koenigl, Astrophys. J. Lett., 370, L39 (1991). https://doi.org/10.1086/185972

28. M. M. Romanova, G. V. Ustyugova, A. V. Koldoba, and R. V. E. Lovelace, Astrophys. J. Lett., 578,

No. 1, 420–438 (2002). https://doi.org/10.1086/342464

29. J. Arons and S. M. Lea, Astrophys. J., 207, 914–936 (1976). https://doi.org/10.1086/154562

30. A. K. Kulkarni and M. M. Romanova, Mon. Not. Roy. Astron. Soc., 386, No. 2, 673–687 (2008).

https://doi.org/10.1111/j.1365-2966.2008.13094.x

31. Yu. P. Raizer, Prikl. Mekh. Tekh. Fiz., No. 6, 19–28 (1963).

32. D.Winske, J. D. Huba, C. Niemann, and A. Le, Front. Astron. Space Sci., 5, 51 (2019).

https://doi.org/10.3389/fspas.2018.00051

33. A. A. Soloviev, K. F. Burdonov, V. N. Ginzburg, et al., Nucl. Instrum. Meth. Phys. Res. A, 653, No. 1,

35–41 (2011). https://doi.org/10.1016/j.nima.2011.01.180

34. K. F. Burdonov, A. A. Eremeev, N. I. Ignatova, et al., Quantum Electron., 46, No. 4, 283–287 (2016).

https://doi.org/10.1070/QEL16043

35. V. V. Lozhkarev, G. I. Freidman, V. N. Ginzburg, et al., Laser Phys. Lett., 4, No. 6, 421–427 (2007).

https://doi.org/10.1002/lapl.200710008

36. A. K. Poteomkin, E. A. Khazanov, M. A. Martyanov, et al., IEEE J. Quantum Electron., 45, No. 7,

854–863. https://doi.org/10.1109/JQE.2009.2013209

37. C. Garban-Labaune, E. Fabre, C. E. Max, et al., Phys. Rev. Lett., 48, No. 15, 1018–1021 (1982).

https://doi.org/10.1103/PhysRevLett.48.1018

38. M. G. Lobok, A. V. Brantov, and V. Yu. Bychenkov, Phys. Plasmas, 26, No. 12, 123107 (2019). https://doi.org/10.1063/1.5125968

39. V. Yu. Bychenkov, M. G. Lobok, V. F. Kovalev, and A. V. Brantov, Plasma Phys. Control. Fusion, 61, No. 12, 124004 (2019). https://doi.org/10.1088/1361-6587/ab5142